Article

Influence of the PAN:PEO Ratio on the Morphology of Needleless Electrospun Nanofiber Mats Before and After Carbonization

Nonsikelelo Sheron Mpofu [1,2] , Yusuf Topuz [1], Elzbieta Stepula [1], Uwe Güth [3], Timo Grothe [1] ,
Jan Lukas Storck [1] , Martin Wortmann [1], Boris Mahltig [4] and Andrea Ehrmann [1,*]

1 Faculty of Engineering and Mathematics, Bielefeld University of Applied Sciences and Arts,
  33619 Bielefeld, Germany; nonsiempofu@gmail.com (N.S.M.); yusuf.topuz@hsbi.de (Y.T.);
  elzbieta.stepula@hsbi.de (E.S.); timo.grothe@hsbi.de (T.G.); jan_lukas.storck@hsbi.de (J.L.S.);
  wortmann@hsbi.de (M.W.)
2 School of Engineering, Moi University, Eldoret 30100, Kenya
3 Department of Physical and Biophysical Chemistry (PC III), Faculty of Chemistry, Bielefeld University,
  33615 Bielefeld, Germany; uwe.gueth@uni-bielefeld.de
4 Faculty of Textile and Clothing Technology, Niederrhein University of Applied Sciences,
  41065 Mönchengladbach, Germany; boris.mahltig@hs-niederrhein.de
* Correspondence: andrea.ehrmann@hsbi.de

Abstract: Nanofiber mats with a high surface-to-volume ratio can be prepared by electrospinning. The Porosity is sometimes reported to be tunable by blending different materials, e.g., water-soluble poly(ethylene oxide) (PEO) with not water-soluble poly(acrylonitrile) (PAN). Here, nanofiber mats were electrospun from different PAN:PEO ratios, using a wire-based electrospinning machine "Nanospider Lab". Investigations of the as-spun nanofiber mats as well as of membranes after washing off the water-soluble PEO by scanning electron microscopy (SEM) revealed severe differences in the nanofiber mat morphologies, such as varying fiber diameters and especially non-fibrous areas in the carbonized nanofiber mats, depending on the amount of PEO in the nanofiber mat as well as the molecular weight of the PEO. Similarly, the ratio and molecular weight of PEO influenced the results of stabilization and carbonization. This paper discusses the possibility of tailoring nanofiber porosity for the potential use of PAN nanofiber mats in tissue engineering, filtration, and other applications.

Keywords: porosity; stabilization; carbonization; polymer blend; nanofiber mat; nanofibrous membrane

1. Introduction

Nanofiber mats can be electrospun from a broad range of polymers and polymer blends as well as embedded nanoparticles [1–3]. The electrospinning process can be performed by different techniques, where needle-based electrospinning is most commonly used, while different needleless techniques have been developed to increase the production speed [4–6].

Typical applications of nanofibers are, e.g., filtration [7,8], biotechnology and biomedicine [9–11], sensors [12,13], or energy applications [14–16]. In many of these applications, a high specific surface area is advantageous for the material performance [17,18]. While nanofibers already have a high specific surface, as compared to larger fibers or layers, this value can be further increased by preparing porous nanofibers.

Several attempts have been described in the literature on how pores can be introduced into nanofibers. A recent overview was given by Liu et al. [19], who described the introduction of micropores, mesopores, and macropores into nanofibers by techniques such as phase separation, calcination of polymer/ceramic or polymer/metal nanofibers, or multi-fluid electrospinning, which can be used only for specific polymers, solvents, or with special electrospinning equipment. A more general approach to gaining porous nanofibers

from not water-soluble polymers is electrospinning in high humidity [20,21]. While this approach has been shown to work well for several polymers, it was not successful for poly(acrylonitrile) (PAN) [22], a polymer that is often used as a carbon precursor due to its high carbon yield. In addition, spinning in high humidity may even impede the electrospinning of PAN, e.g., in the case of wire-based electrospinning of PAN dissolved in dimethylsulfoxide (DMSO), a low-toxic solvent, which is thus preferable for medical applications [23–25].

Another possibility to produce porous nanofibers is given by combining water-soluble with not water-soluble polymers and removing the first by washing after electrospinning. This process was reported, e.g., for chitosan blended with poly(ethylene oxide) (PEO) in different ratios, leading to porous chitosan nanofibers after washing out the PEO for 1 h [26].

On the other hand, carbonization was used as a method to gain porous carbon nanofibers from electrospun polymer blends, such as lignin/poly(vinyl pyrrolidone) (PVP) [27]. To prepare porous carbon nanofibers from PAN, often Si-containing compounds are added, such as tetraethyl orthosilicate (TEOS), poly(methyl hydrosiloxane) (PMHS), or phenylsilane [28]. Blending PAN with polymethyl methacrylate (PMMA) and subsequent stabilization and carbonization also resulted in porous carbon nanofibers [29]. Another possibility to prepare porous carbon nanofibers from PAN is given by adding graphene nanosheets or carbon nanotubes in the spinning solution [30,31]. Electrospinning pure PAN nanofibers, followed by stabilization, carbonization, and, finally, activation by adding steam to the nitrogen flow in the carbonization oven also resulted in porous carbon nanofibers [32]. Electrospinning of PAN/FeC_2O_4, followed by stabilization and carbonization as well as thermal treatment in NH_3 at 800 °C for 1 h resulted in highly porous Fe-N/carbon nanofibers [33].

A polymer blend that is often mentioned in the literature regarding porous PAN or carbon fibers is PAN/PEO. Zhang and Hsieh used needle-based electrospinning of PAN (150 kDa) with PEO (10 kDa) in a ratio 1:1 dissolved in dimethylformamide (DMF) to gain carbon nanofibers with a rough surface, but without visible pores, and a smaller diameter than carbon nanofibers from pure PAN [34]. In a previous study using identical polymers, they showed the effect of water treatment to wash out the PEO from PAN/PEO nanofibers mixed in ratios of 50:50 or 70:30, resulting in indents and ridges along the fiber surface [35]. On the other hand, Yang et al. showed highly porous carbon nanofibers prepared by needle-based electrospinning of PAN (molecular weight 150 kDa) with PEO (300 kDa) from DMF if the PAN:PEO ratio was 1:1 or 1:2 [36].

These different results may be attributed to the different molecular weights of the PEO used in these experiments. Other electrospinning systems or solvents, however, have not been taken into account yet in studies regarding PAN/PEO nanofibers.

Here, we report the effect of adding PEO in different ratios and with varying molecular weight to PAN solutions prepared with the low-toxic solvent DMSO, electrospun with the wire-based "Nanospider" system, stabilized, and carbonized. Investigations of wire-based electrospinning of PAN:PEO nanofiber mats from DMSO have, to the best of our knowledge, not been reported before in the scientific literature and are necessary for a comparison with the aforementioned reports on needle-based electrospinning from DMF. To characterize nanofiber mats and single nanofibers regarding their regularity and potential porosity, respectively, microscopic techniques with different magnifications are used, from confocal laser microscopy (CLSM) to scanning electron microscopy (SEM) to atomic force microscopy (AFM).

2. Materials and Methods

Electrospinning solutions were prepared from PAN (X-PAN copolymer, consisting of 93.5% acrylonitrile, 6% methylacrylate, and 0.5% sodium methallyl sulfonate, produced by Dralon, Dormagen, Germany; molecular weight 250 kDa) in DMSO (min. 99.9%, S3 chemicals, Bad Oeynhausen, Germany). In addition to pure PAN, PAN:PEO blends were dissolved in DMSO, keeping a solid content of 16%. Different PAN:PEO ratios of 9:1,

8:2, 7:3, and 6:4 were chosen, where the last was nearly unspinnable, so that no further ratios were tested. PEO with different molecular weights (40 kDa, 300 kDa, 600 kDa, and 1000 kDa, Sigma-Aldrich, Saint Louis, MO, USA) was used in the experiments. Solutions were prepared by constant stirring with 200 rpm for 1 day at a temperature of 40 °C.

The wire-based electrospinning device "Nanospider Lab" (Elmarco Ltd., Liberec, Czech Republic) was used to prepare nanofiber mats. Most spinning parameters were kept constant, as follows: relative humidity 32–33%, carriage speed 100 mm/s, substrate speed 0 mm/min, electrode–electrode distance 240 mm, ground electrode–substrate distance 50 mm, nozzle diameter 0.9 mm, and duration 30 min. The voltage was slightly modified to optimize the spinning process, while the current and temperature in the spinning chamber could not be controlled. These parameters are given in Table 1 for the samples under investigation.

Table 1. Varying electrospinning parameters. The first column gives mixing ratios and the molecular weight of the included PEO.

Sample	Voltage/kV	Current/mA	Temperature/°C
PAN:PEO 9:1, 40 kDa	60	0.035	21.3
PAN:PEO 9:1, 300 kDa	60	0.03	22.4
PAN:PEO 9:1, 600 kDa	60	0.02	24.6
PAN:PEO 9:1, 1000 kDa	70	0.055	21.5
PAN:PEO 8:2, 300 kDa	70	0.05	23.6
PAN:PEO 7:3, 300 kDa *	70	0.07 (0.06)	24.4 (23.1)
PAN:PEO 6:4, 300 kDa *	70	0.1 (0.06)	23.4 (24.0)
Pure PAN	65	0.035	23.4

* These experiments were repeated at slightly different temperatures (in brackets).

Stabilization of parts of these samples was performed in a muffle oven B150 (Nabertherm, Lilienthal, Germany) by approaching a stabilization temperature of 280 °C with a heating rate of 1 K/min, followed by isothermal treatment for 1 h. The stabilized samples were carbonized in a tube furnace CTF 12/TZF 12 (Carbolite Gero Ltd., Sheffield, UK) at 500 °C for 1 h, approached by a heating rate of 5 K/min, in a constant nitrogen flow of 100 mL/min (STP). These heating rates and temperatures correspond to previous studies to enable comparison [37,38]. Sample masses were taken with an analytical balance (VWR, Radnor, PA, USA).

Surface investigations of the nanofiber mats were performed by CLSM (VK-8710, Keyence, Neu-Isenburg, Germany), SEM (Phenom ProX G3 Desktop SEM, Thermo Fisher Scientific, Waltham, MA, USA), and AFM (FlexAFM, Nanosurf, Liestal, Switzerland, using a Tap 190 Al-G cantilever in the dynamic mode).

The nanofiber diameters were measured on the SEM images using ImageJ (version 1.53e, 2021, National Institutes of Health, Bethesda, MD, USA), taking into account 100 arbitrarily chosen fibers per specimen.

The effect of watering the electrospun samples for different durations on the amount of PEO in them was investigated by differential scanning calorimetry (DSC 3, Mettler-Toledo, Gießen, Germany).

Raman microscopy was conducted utilizing a WITec alpha300 apyron (Ulm, Germany). The spectra were acquired using a 532 nm laser with a power output of 10 mW, an integration time of 3 s, and a 50× objective. Spectral data processing was performed using the software WITec Project SIX 6.2.10.147 (WITec, Ulm, Germany).

Fourier-transform infrared (FTIR) spectroscopy was measured by an IRTracer-100 (Shimadzu, Kyoto, Japan), using 40 scans with a resolution of 1 cm^{-1}. This IR spectrometer is equipped with a Specac Golden Gate ATR unit.

X-ray diffractometry (XRD) measurements were performed with an X'Pert Pro MPD PW3040-60 diffractometer (Malvern Panalytical GmbH, Kassel, Germany) using Cu Kα radiation (λ = 1.54056 Å).

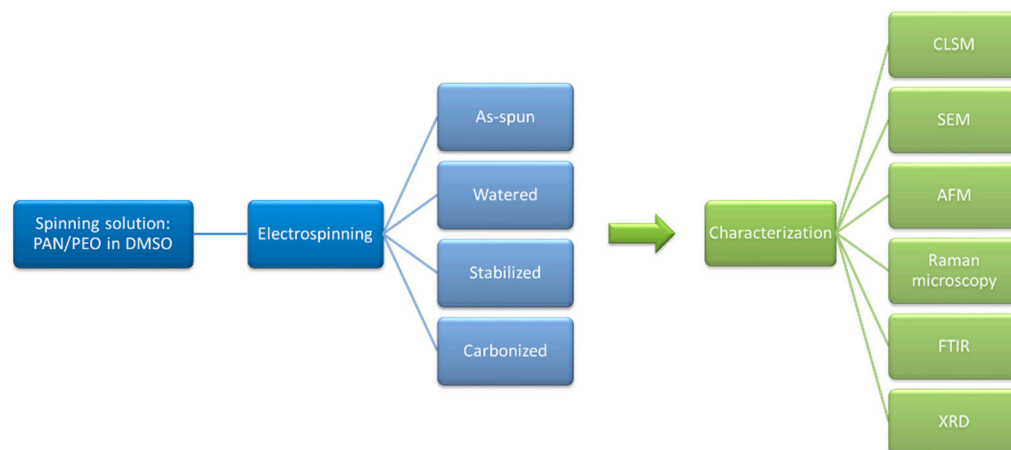Figure 1 shows a schematic representation of the working plan.

Figure 1. Schematic of the working plan.

3. Results and Discussion

3.1. Comparison of As-Spun Samples

Firstly, PAN:PEO nanofiber mats with different blend ratios and varying PEO molecular weights were investigated regarding their spinnability and the general nanofiber mat morphology. A comparison of samples prepared with a PAN:PEO ratio of 9:1 and different PEO molecular weights is given in Figure 2, based on SEM images with identical magnification of $5000\times$. SEM images with lower magnification ($1000\times$) as well as CLSM images can be found in the Supplementary Information (Figures S1 and S2). Generally, all nanofiber mats look similar, besides the one prepared with PEO 600 kDa (Figure 2c), which exhibits a large number of broken fibers, beads, and other non-fibrous structures. A possible explanation for this finding is the relatively high temperature during spinning (cf. Table 1), while a general problem with this specific PEO cannot be excluded.

For PEO with a molecular weight of 300 kDa, more mixing ratios were tested. This molecular weight was chosen since the nanofiber mats with PEO 40 kDa were very thin and irregularly spun with non-fibrous areas visible in CLSM (Figure S2), PEO 600 kDa led to broken fibers and an unusually high number of beads (Figure 2c), and PEO 1000 kDa showed undesired "cotton candy" formation during electrospinning so that PEO 300 kDa can be assumed to be best spinnable. In addition, PAN:PEO solutions with PEO 300 kDa had the longest shelf life of several weeks, while all other solutions were solidified or unmixed after around two weeks.

SEM images of these nanofiber mats are depicted in Figure 3 for a nominal magnification of $5000\times$ and in Figures S3 and S4 for smaller nominal magnifications. While the PAN:PEO ratio of 6:4 shows a highly porous mat with only a few fibers (Figure 3c), as already mentioned before based on the optical appearance of the nanofiber mat, the ratio 7:3 (Figures 3b and S3b) unexpectedly shows fibers with a much larger diameter. This may again be attributed to a higher temperature during spinning (cf. Table 1) since all other solution and spinning parameters were identical with the samples with other ratios. To test this idea, the solutions with PAN:PEO 7:3 and 6:4 were again electrospun at slightly different temperatures (cf. Table 1), leading to significantly thinner fibers for PAN:PEO 7:3 at a lower temperature and slightly increased fiber diameters for PAN:PEO 6:4 spun at a higher temperature.

Raman microscopy was used to chemically analyze the samples. Initially, pure reference spectra of PAN and PEO powders were obtained, revealing the characteristic bands associated with these two compounds (Figure 4a). Subsequently, a pure PAN nanofiber mat was examined under the microscope, where a small area (Figure 4b) was scanned with an integration time of 3 s. A Raman false-color image was generated using a sum filter based on the peak observed at $1460 \text{ cm}^{\times 1}$, illustrating the heterogeneity of the compound within the mat (Figure 4c).
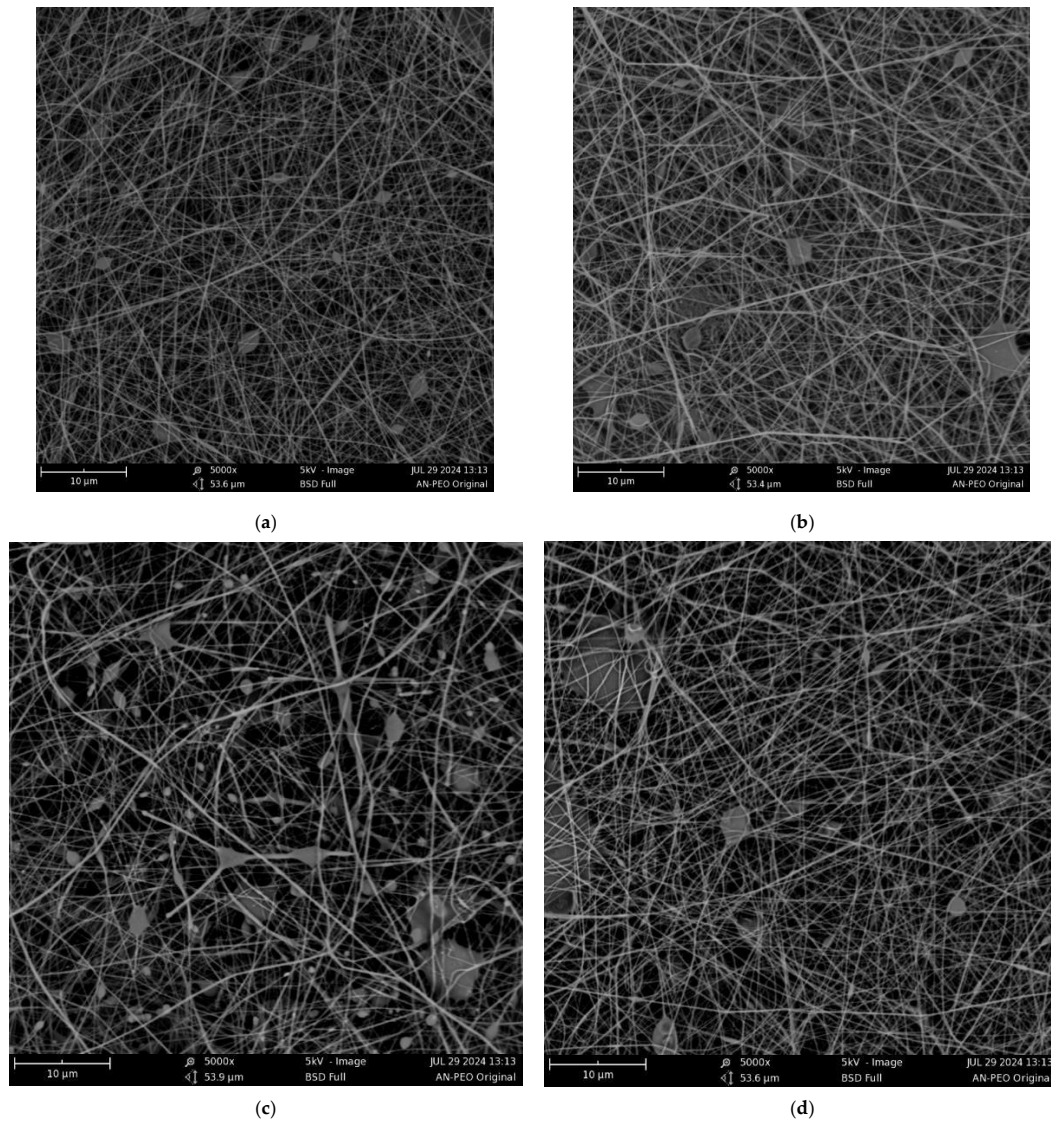
Figure 2. Scanning electron microscopy (SEM) images with nominal magnification $5000\times$ of PAN:PEO 9:1, PEO molecular weight: (**a**) 40 kDa; (**b**) 300 kDa; (**c**) 600 kDa; (**d**) 1000 kDa.
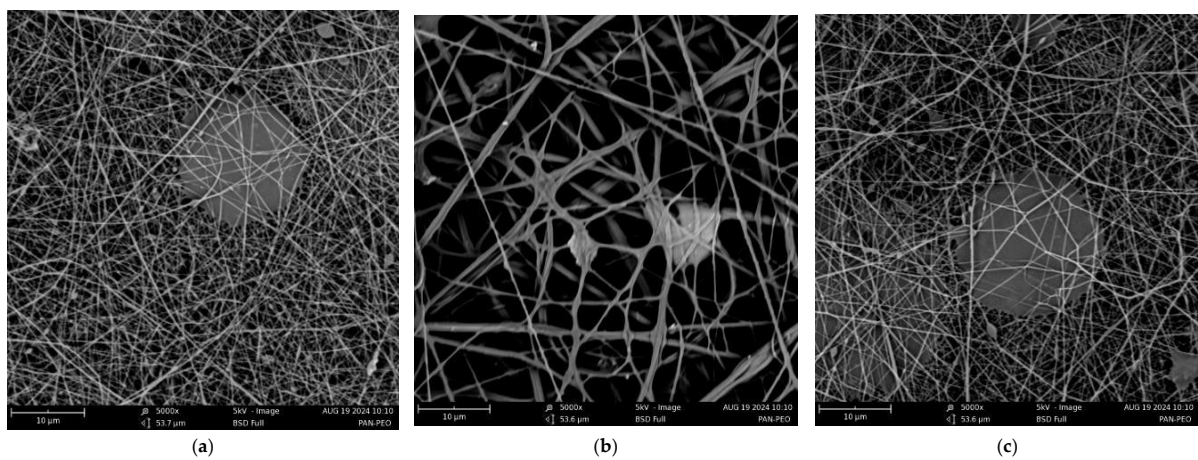

Figure 3. Scanning electron microscopy (SEM) images with nominal magnification $5000\times$ of PAN:PEO mixing ratios: (**a**) 8:2; (**b**) 7:3; (**c**) 6:4, using PEO with molecular weight 300 kDa.
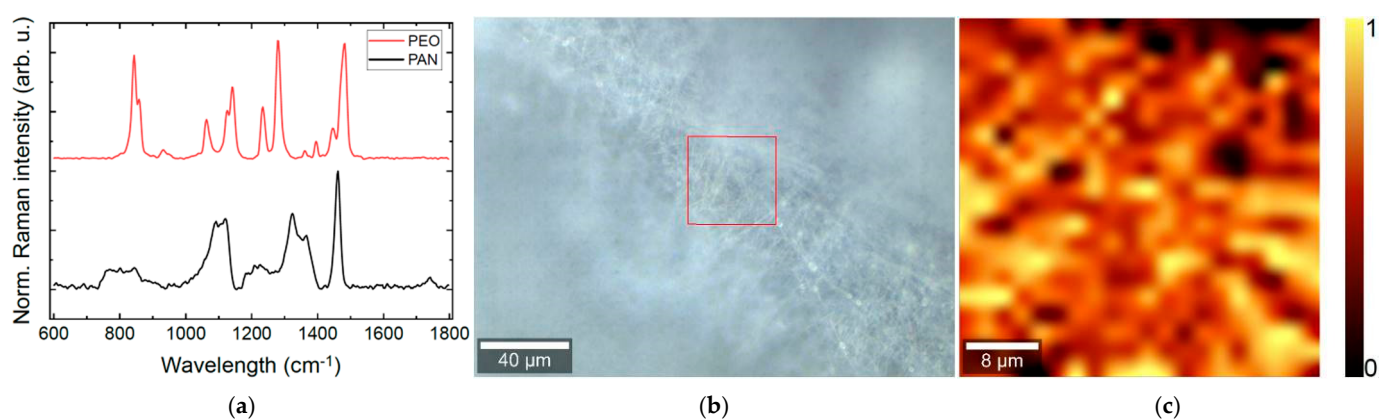
Figure 4. (**a**) Raman reference spectra of PAN and PEO; (**b**) microscopic image of PAN nanofiber mat with red square indicating the area of (**c**) a Raman false-color image.

Following this, a PAN:PEO 9:1 sample was analyzed (Figure 5a). Again, a localized area of the sample was scanned, leading to the creation of two Raman false-color images through univariate analysis. The first false-color image corresponded to PAN, while the second was attributed to PEO. These images indicated that the predominant region comprised PAN, with only a minor area consisting of PEO. This will be discussed further in correlation with the FTIR measurements on this sample.
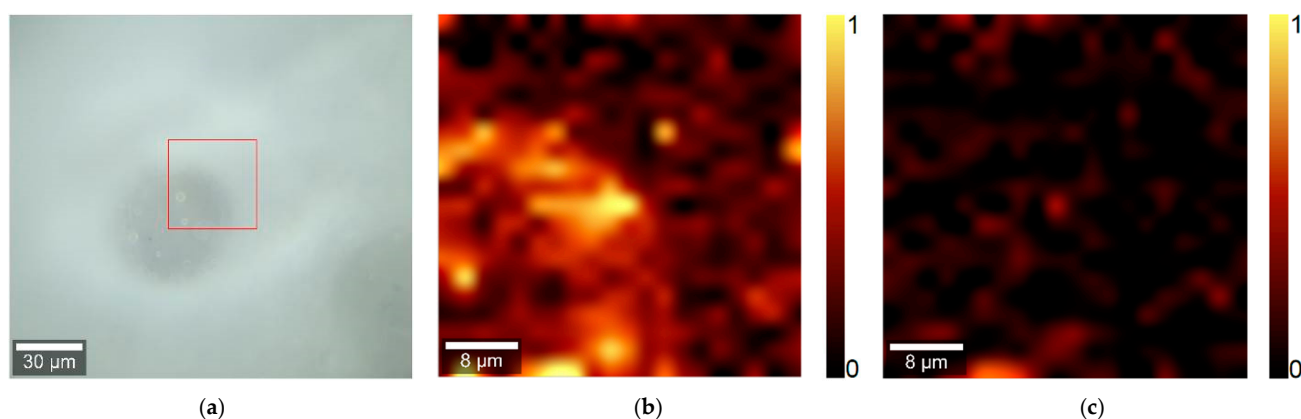

Figure 5. (**a**) PAN:PEO 9:1 nanofiber mat with red square marking the area of Raman microscopy images; (**b**) PAN abundance image; (**c**) PEO abundance image.

3.2. Effect of Watering the Samples

In this paper, mainly the effect of PEO on PAN nanofiber mats and nanofibers should be investigated after washing the PEO out of the nanofiber mat or after carbonization to enable full thermal degradation of PEO, which happens around 400 °C, with the exact temperature range depending on the molecular weight [39–41], i.e., below the chosen carbonization temperature of 500 °C.

Figure 6 thus compares CLSM images of PAN:PEO 9:1 with PEO 300 kDa as-spun and after watering for 1 min or 21 h as well as corresponding DSC measurements. Generally, on this scale, some irregularities are visible in the nanofiber mats, which increase upon watering (Figure 6a–c). It should be mentioned that the DSC measurement (Figure 6d) reveals that PEO with a melting point near 65 °C [40–42], depending on the molecular weight, is reduced after 1 min of watering and mostly vanishes after 21 h of watering. This indicates that the brighter, less fibrous areas especially visible in Figure 6c stem from washed-out PEO.
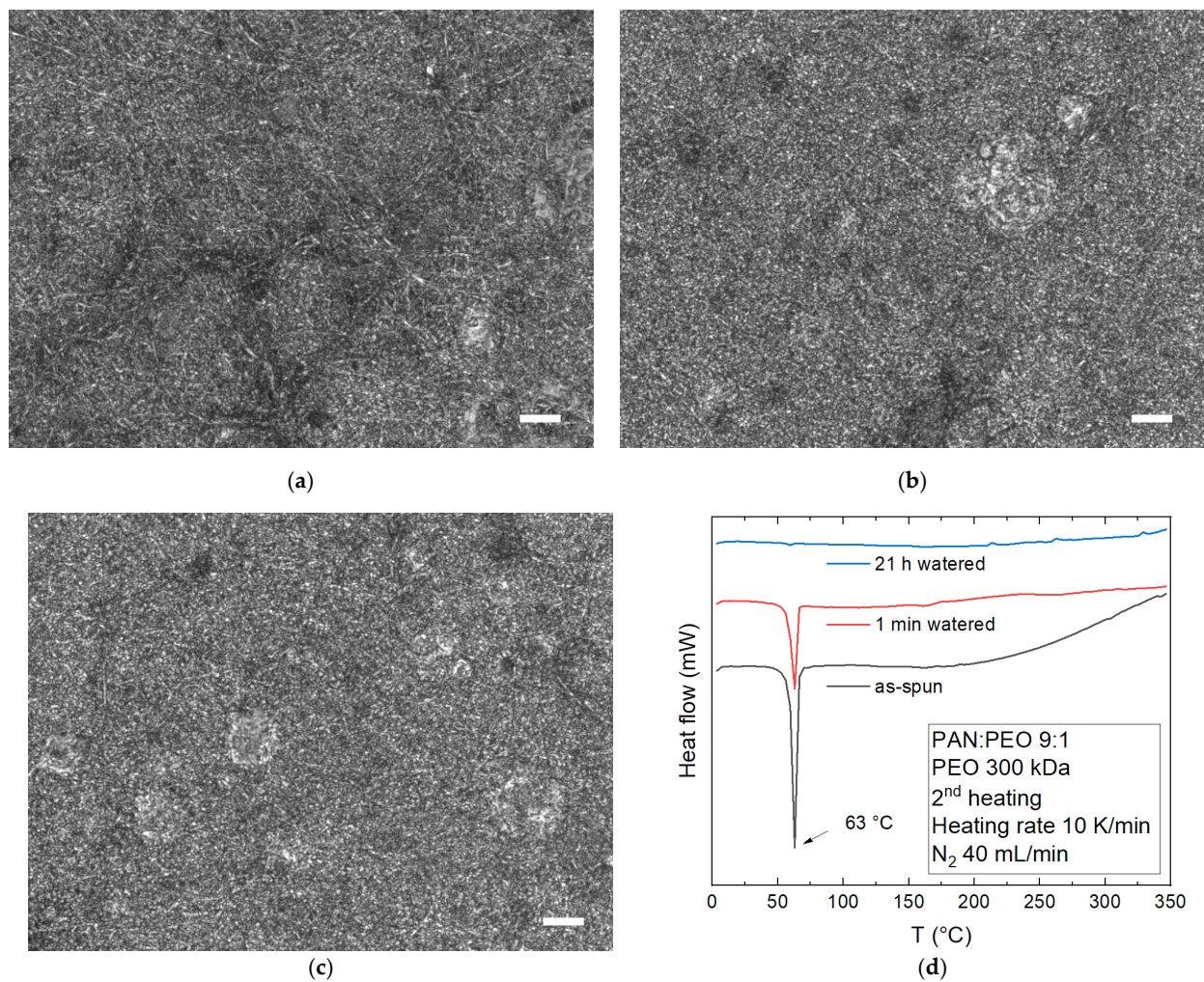
Figure 6. PAN:PEO 9:1, with PEO 300 kDa: CLSM images of (**a**) as-spun sample; (**b**) sample watered for 1 min; (**c**) sample watered for 21 h; (**d**) DSC measurement of these samples. Scale bars correspond to 1 μm.

While washing apparently influences the nanofiber mats on relatively large scales, a comparison on smaller scales is given in Figure 7. Comparing the SEM images of the as-spun (Figure 7a) and watered samples (Figure 7c), no differences are visible. Similarly, the AFM images of both samples (Figure 7b,d) do not show any obvious differences. In particular, there are no pores in the fibers visible after watering for 21 h (Figure 7d). While Yang et al. [36] found pores in PAN:PEO nanofiber mats using PEO with the same molecular weight of 300 kDa as in the sample investigated here, they used samples with a much higher ratio of PEO (50% or 67% of the solid content), which could not be tested in our wire-based electrospinning device where a PEO ratio of 40% of the solid content already resulted in a very thin, irregular nanofiber mat.
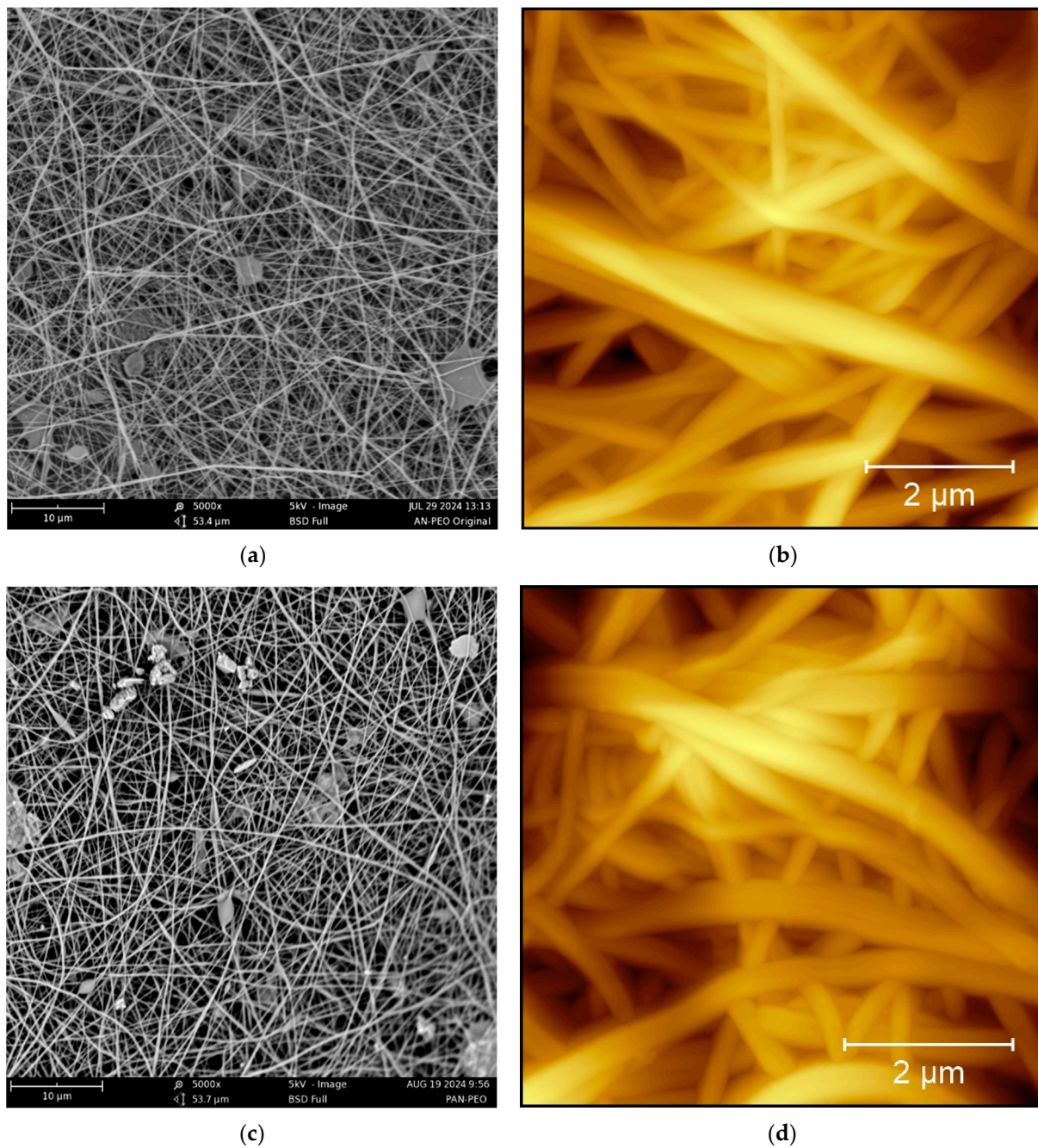
Figure 7. PAN:PEO 9:1, with PEO 300 kDa: as-spun, images by (**a**) SEM and (**b**) AFM; watered for 21 h, images by (**c**) SEM and (**d**) AFM.

Similarly to the sample with PEO 300 kDa, no differences in the fiber surface could be measured by AFM in the other samples with PAN:PEO ratio of 9:1, as shown in Figure 8 (AFM images) and Figure S5 (SEM images). Here, again, no clear differences are visible between as-spun and samples watered for 1 min, and, in particular, no pores can be found in the watered samples. Next, the impact of stabilization and carbonization on these samples is investigated.
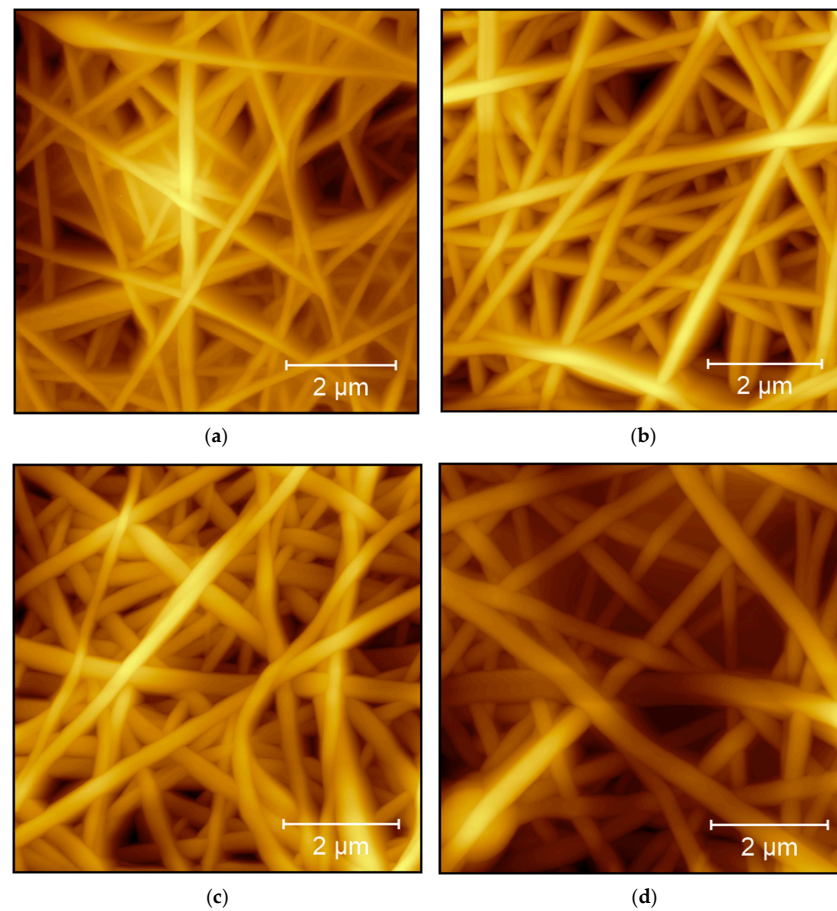
Figure 8. AFM images before (upper row) and after watering (lower row) of PAN:PEO 9:1 samples with different PEO molecular weights: (**a**) 40 kDa as-spun; (**b**) 1000 kDa as-spun, (**c**) 40 kDa watered for 1 min; (**d**) 1000 kDa watered for 1 min.

The chemical analysis of the nanofiber mats was performed by Raman microscopy (Figures 4 and 5) and FTIR. FTIR measurements are depicted in Figure 9. PAN powder as well as the pure PAN nanofiber mat show the typical spectrum of a PAN copolymer [43]. Prominent PAN peaks can be found at 2939 cm^{-1}, 1451 cm^{-1}, and 1363 cm^{-1} (C-H$_2$ bending and stretching) as well as 2243 cm^{-1} (C≡N stretching vibration) [43,44]. The peak at 1734 cm^{-1} is typical for a PAN copolymer and can probably be attributed to the C=O stretching vibration, which may stem from an ester group in a co-monomer unit [43].
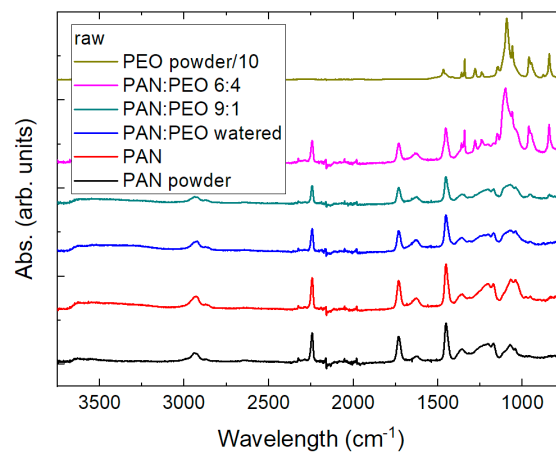

Figure 9. FTIR measurements of raw electrospun nanofiber mats as well as pure powders (spectrum of PEO powder divided by 10).

The PEO powder spectrum allows for the identification of typical peaks such as 1467 cm^{-1} (asymmetric CH$_2$ bending), 1342 cm^{-1} (CH$_2$ wagging of amorphous PEO), 1093 cm^{-1} (asymmetric –C–O–C– stretching), 961 cm^{-1} (CH$_2$ twisting), and 841 cm^{-1} (CH$_2$ wagging) [45–47].

While the PAN:PEO 6:4 sample shows the expected superposition of PAN and PEO peaks, unexpectedly, the PEO peaks nearly completely vanished in PAN:PEO 9:1, even in the as-spun sample and not only in the watered one where PEO could be expected to be washed out. This finding may be attributed to the separation of both polymers during the spinning process and thus to larger areas mainly consisting of PAN and smaller areas mainly consisting of PEO. This finding corresponds to the results of Raman microscopy on the PAN:PEO 9:1 sample, as discussed before.

3.3. Stabilization and Carbonization

After stabilization and carbonization, pure PAN samples become brown and dark gray/black, respectively, as depicted in Figure 10. For the here chosen relatively low carbonization temperature of 500 °C, carbonization will not be completed, resulting in slightly brownish fibers after this incipient carbonization instead. This behavior is typical for the oxidative stabilization process and the subsequent carbonization, respectively [37,38].
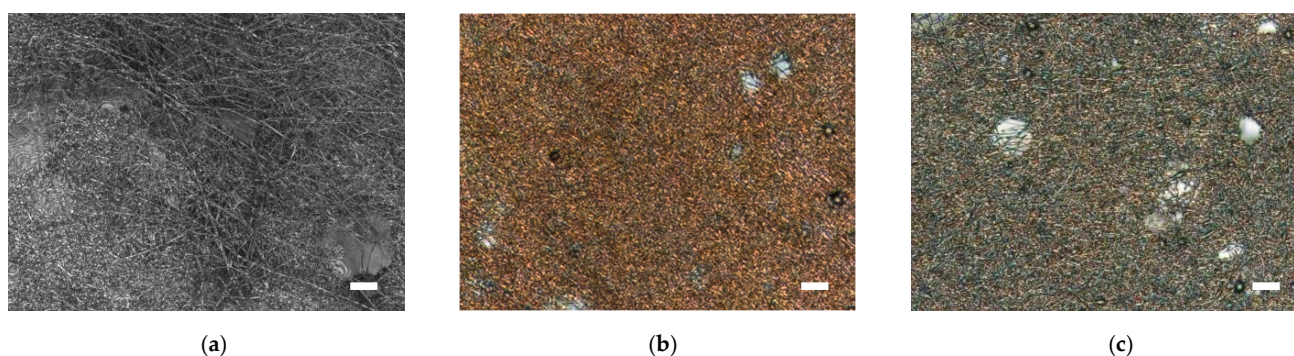

(a)   (b)   (c)

Figure 10. CLSM images of pure PAN reference samples: (**a**) as-spun; (**b**) stabilized; (**c**) carbonized. Scale bars correspond to 1 μm.

Interestingly, this is different for PAN:PEO blended samples, where stabilized samples become darker with an increasing amount of PEO (Figure 11). While samples with 90% PAN are nearly fully brown after stabilization (Figure 11a), dark-gray areas become visible for the samples with 20% PEO (Figure 11b), while the sample with the highest amount of PEO has largely dark-gray non-fibrous areas with brown fibrous regions embedded (Figure 11d). Interestingly, the sample with PAN:PEO 7:3 (Figure 11c) shows brown as well as dark-gray fibers, suggesting that thicker PEO fibers can withstand the stabilization process in spite of the PEO melting point (~63 °C) being much lower than the stabilization temperature. The clear difference between brown and dark-gray fibers further suggests that the difference between this sample and the others is not related to better mixing of the polymers, but has to be related to a difference in the spinning process.

Comparing the stabilization processes of PAN:PEO samples with a ratio of 9:1 and different PEO molecular weights, Figure 12a shows a large amount of dark-gray PEO "isles" for PEO 40 kDa, while PEO 600 kDa (Figure 12b) leads to a relatively homogeneous result after stabilization, and PEO 1000 kDa (Figure 12c) shows clear inhomogeneities where PEO forms rounded lines. This supports the previous choice PEO 300 kDa as ideal for these tests.
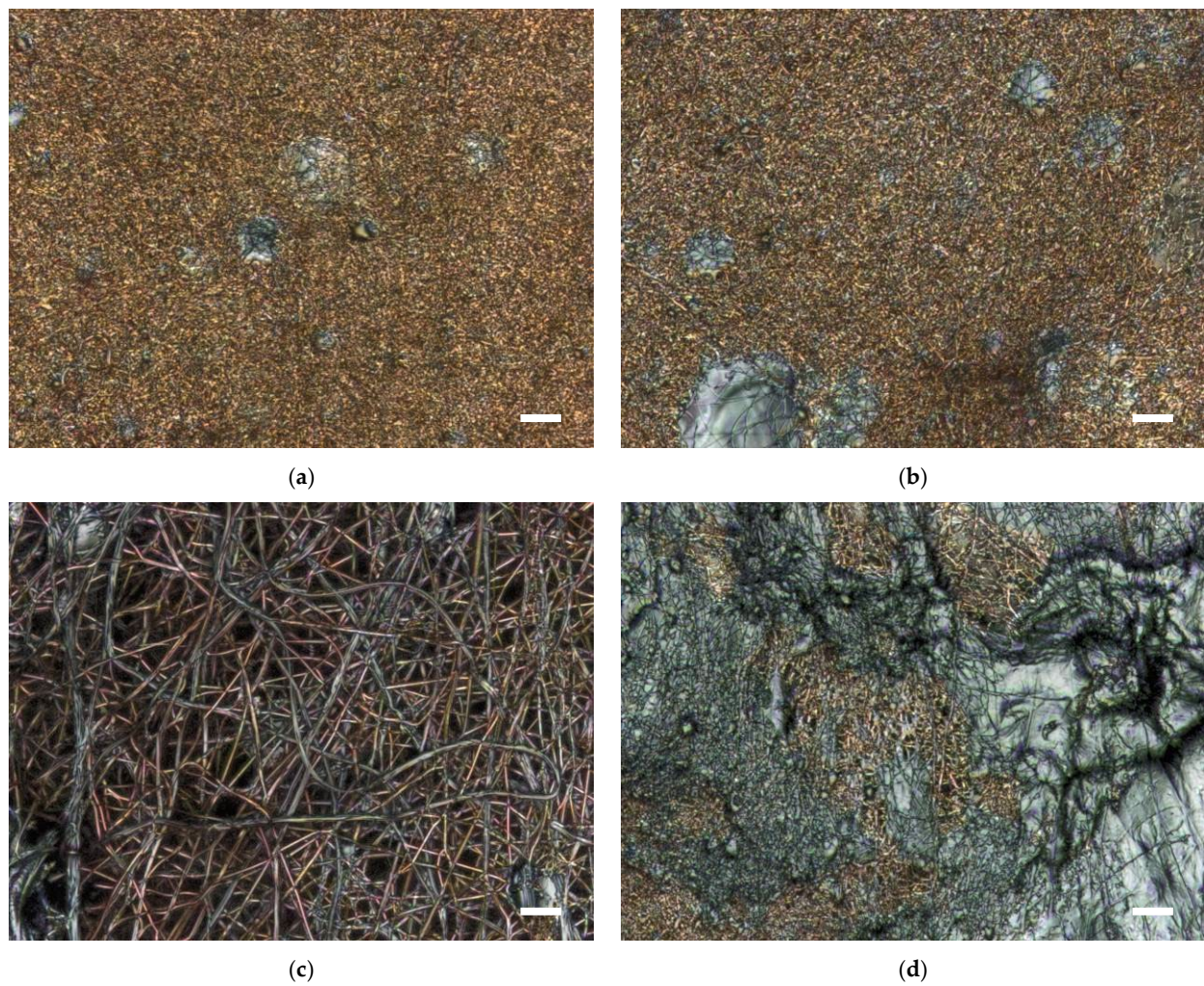
Figure 11. CLSM images of PAN:PEO samples after stabilization with a PAN:PEO ratio of (**a**) 9:1; (**b**) 8:2; (**c**) 7:3; (**d**) 6:4 and PEO 300 kDa. Scale bars correspond to 1 μm.
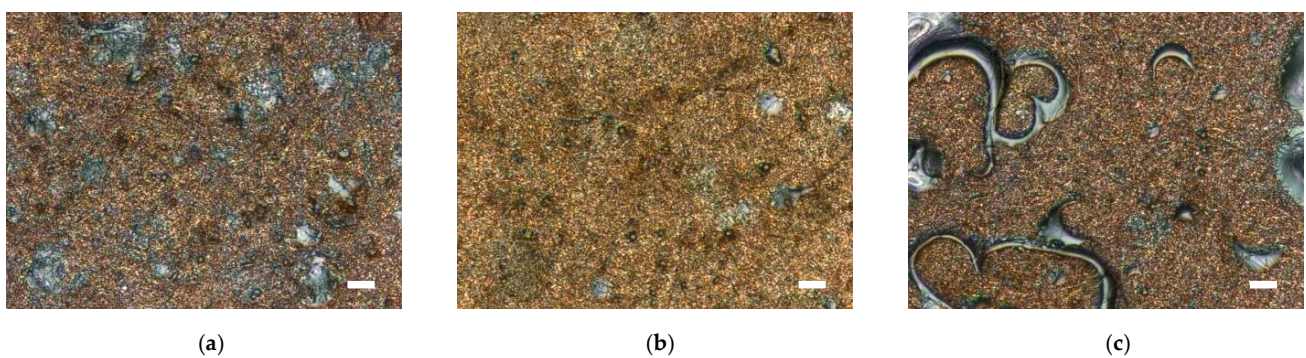

Figure 12. CLSM images of PAN:PEO samples after stabilization with a PAN:PEO ratio of 9:1 and PEO molecular weights of (**a**) 40 kDa; (**b**) 600 kDa; (**c**) 1000 kDa. Scale bars correspond to 1 μm.

Going one step further, Figure 13 shows CLSM images of carbonized samples with different amounts of PEO 300 kDa. While PAN:PEO 9:1 reveals a mostly fibrous sample with only a small non-fibrous area (Figure 13a), more non-fibrous areas are visible for the 8:2 blend (Figure 13b), and even a large part of the 6:4 sample is non-fibrous (Figure 13d). On the other hand, no non-fibrous areas are visible in the 7:3 sample (Figure 13c), similar to Figure 11c. This finding is unexpected since the carbonization temperature of 500 °C is higher than the usually reported degradation temperatures of PEO [39–41]. However,

there are reports in the literature that PEO can indeed also be carbonized [48], although with lower efficiency than PAN [49]. While the stabilization step is mandatory for the carbonization of PAN, PEO in different blends with chitosan could even be carbonized in a one-step process under N_2 flow to obtain carbon nanofibers [49,50]. Alternatively, nanofibers electrospun from NaH_2PO_4, NH_4VO_3, citric acid, and PEO can be carbonized at 500 °C under the Ar atmosphere [51]. The here visible non-fibrous areas have not been found in the literature. A simple explanation for this difference could be that usually the best parts of the produced nanofiber mats are shown in a paper, while the here shown arbitrarily chosen larger areas impede such "cherry-picking" [52].
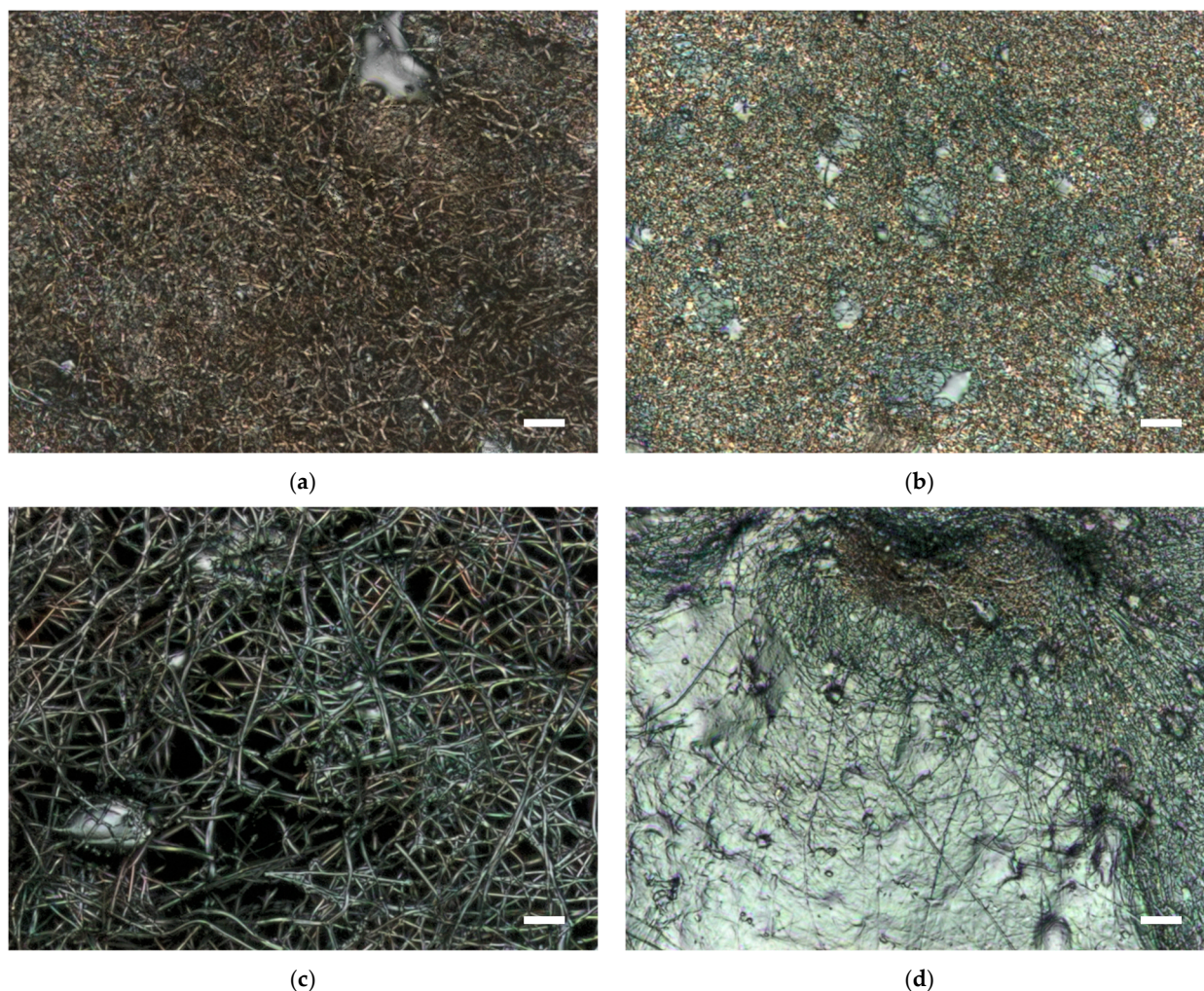

Figure 13. CLSM images of PAN:PEO samples after carbonization with a PAN:PEO ratio of (**a**) 9:1; (**b**) 8:2; (**c**) 7:3; (**d**) 6:4 and PEO 300 kDa. Scale bars correspond to 1 µm.

By comparing the stabilized (Figure 11) and carbonized samples (Figure 13), it is obvious that the formation of non-fibrous areas happens already during the stabilization process. One possibility to avoid this problem may be given by stabilization under an inert gas atmosphere, as described in [49–51]; however, this would impede the stabilization of PAN, which necessitates oxygen. To explain the difference to the nanofibers reported in [34–36] where no large non-fibrous areas were shown, the different electrospinning processes—needle-based in [34–36] and wire-based in this study—have to be taken into account. Such deviations may manifest in different mixing of the polymer solution in the syringe/carriage, different electric fields in both techniques (typically 1 kV/cm for needle-based electrospinning; here, 2.5–3 kV/cm), potentially different spinning durations, temperatures or humidities. Further parameters such as the needle length in needle-based

electrospinning also have an impact on the spinning process, but are not always given in the literature.

A comparison of the other carbonized samples is shown in Figure 14. The samples look very similar to the stabilized ones shown in Figure 12, with 1000 kDa now again having silvery round areas (Figure 14c) instead of the rounded lines visible after stabilization (Figure 14b). This difference can be attributed to investigating different randomly selected areas on the nanofiber mat. For all samples, the SEM images taken after stabilization and carbonization, corresponding to Figures 11–14, can be found in Figures S4–S7.
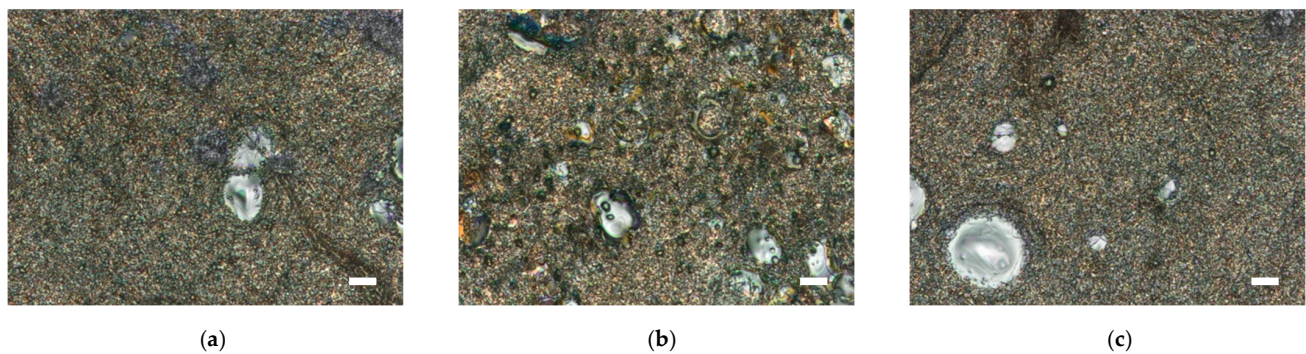

(a)   (b)   (c)

Figure 14. CLSM images of PAN:PEO samples after carbonization with a PAN:PEO ratio of 9:1 and PEO molecular weights of (**a**) 40 kDa; (**b**) 600 kDa; (**c**) 1000 kDa. Scale bars correspond to 1 μm.

Based on the SEM images of the stabilized and carbonized nanofiber mats (Figures S6–S9), Figure 15 depicts exemplarily the nanofiber diameter distributions for a pure PAN nanofiber mat and PAN:PEO 9:1 (300 kDa). While the nanofiber diameter of the PAN nanofiber mat decreases with each thermal treatment, the average diameter remains approximately constant for the PAN:PEO 9:1 (300 kDa) sample during stabilization and carbonization.
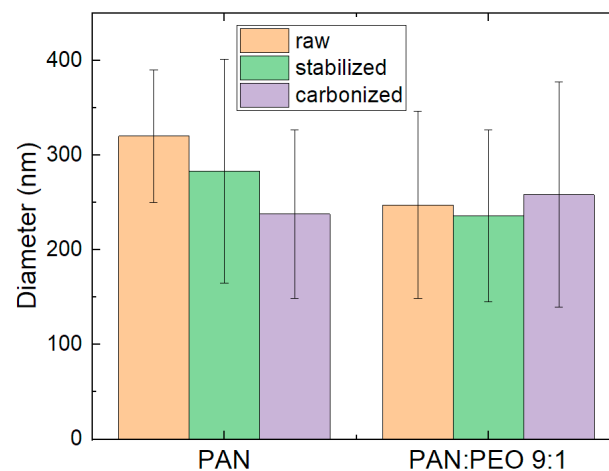

Figure 15. Diameter distribution of pure PAN and PAN:PEO 9:1 (300 kDa) nanofiber mats.

Exemplary AFM images of samples after stabilization and carbonization can be found in Figure 16. The stabilized and carbonized fibers look very similar to the as-spun ones, besides the 7:3 sample with its thicker fibers. It should be mentioned that for the AFM images, fibrous regions on the samples were chosen, while CLSM and SEM images were taken on arbitrary sample areas.
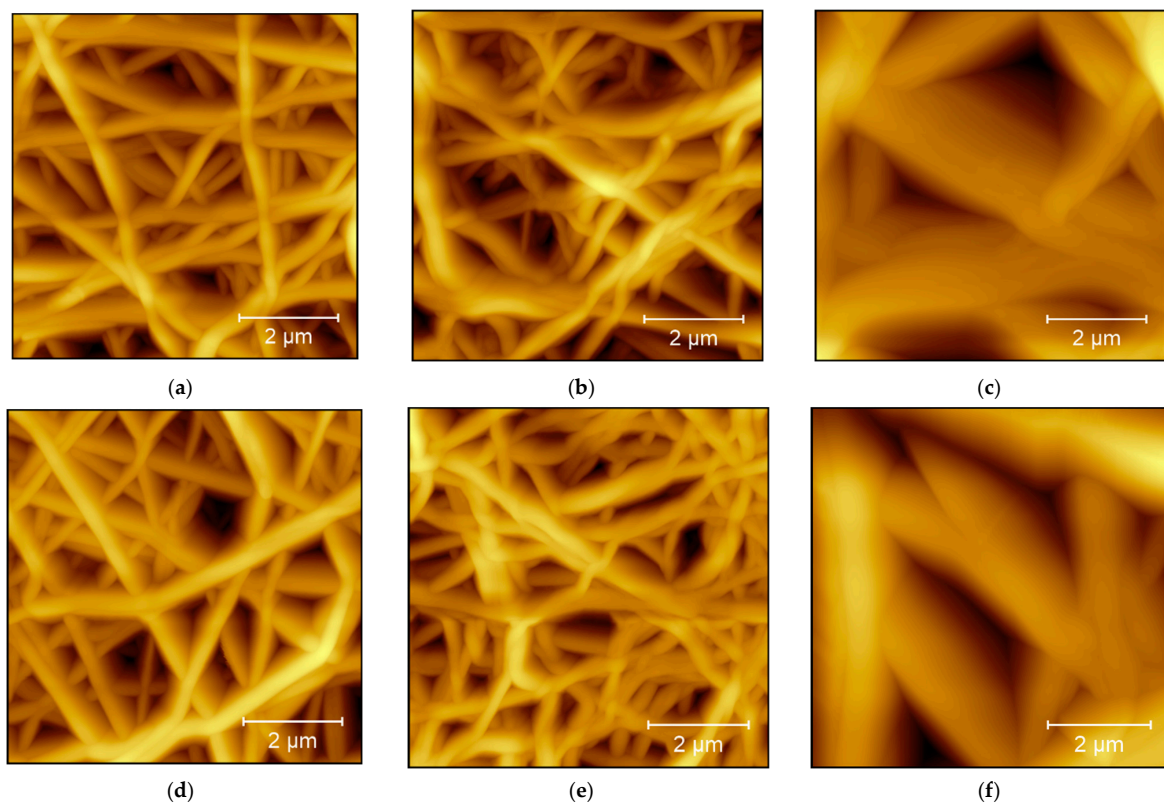
Figure 16. AFM images of PAN:PEO samples after stabilization (upper row) and carbonization (lower row) of different samples: (**a,d**) pure PAN; (**b,e**) PAN:PEO 9:1, PEO 300 kDa; (**c,f**) PAN:PEO 7:3, PEO 300 kDa.

The chemical investigation of the stabilized and carbonized nanofiber mats was performed by Raman microscopy and FTIR. Figure 17a shows the FTIR spectra of the stabilized PAN in comparison with PAN:PEO samples in two different blend ratios. Generally, stabilization leads to a reduction in the nitrile (C≡N) and carbonyl (C=O) peaks, while new peaks occur due to C=N (1576 cm^{-1}) and C=C stretching vibrations (weakly visible around 1660 cm^{-1}), indicating the cyclization–aromatization of the polymers [53]. The peak at 801 cm^{-1} is related to aromatic C–H vibrations, while the peak around 1354 cm^{-1} shows C–H bending and C–H$_2$ wagging [53]. The peak around 1239 cm^{-1} stems from oxygen cross-linking between the polymer chains and indicates C–O vibrations [53]. For PAN:PEO 6:4, the latter seems to be broadened due to superposition with the strongest PEO peak at 1093 cm^{-1}.
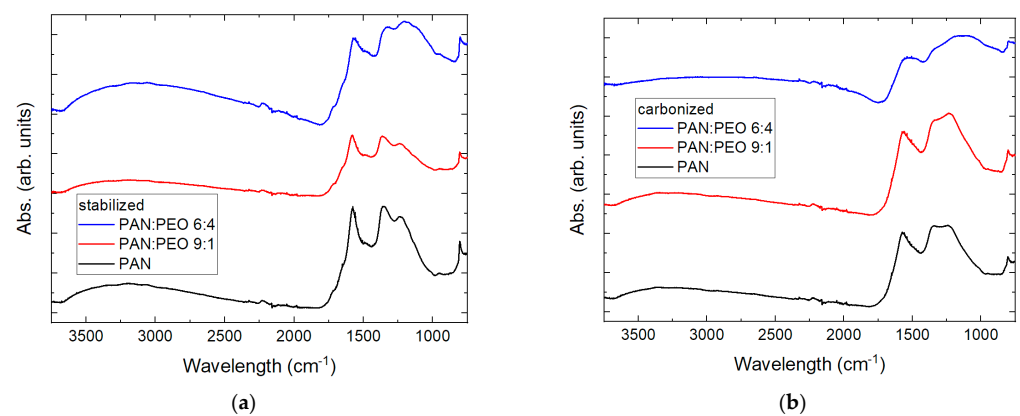

Figure 17. FTIR measurements of (**a**) stabilized and (**b**) carbonized samples.

The carbonized samples (Figure 17b) show relatively large signals, indicating that carbonization is not finished, as pure carbon is chemically almost inert and thus does not show any peaks [54,55]. Here, again, a clear difference between PAN:PEO 6:4 and both other samples is visible, as was also the case for stabilized and raw samples.

The stabilized and carbonized materials were also examined under the Raman microscope, focusing on small areas of the samples that exhibited distinct circular patterns (Figure 18). For each of the three samples, we successfully differentiated between areas with lower and higher ratios of D (@ 1320 cm^{-1}) and G (@ 1560 cm^{-1}) bands in the carbon spectrum. The regions with a higher D/G ratio were highlighted in the false-color images using yellow coloration. Overall, these yellow patterns in the false-color images correlated well with the observed patterns in the wide-field images. These findings suggest the presence of regions within the mat that exhibit a greater number of defects or a higher degree of disorder, which could potentially influence the properties of the nanofiber mat. These areas of higher degree of disorder are identical to the non-fibrous areas, as visible in the microscopic images.
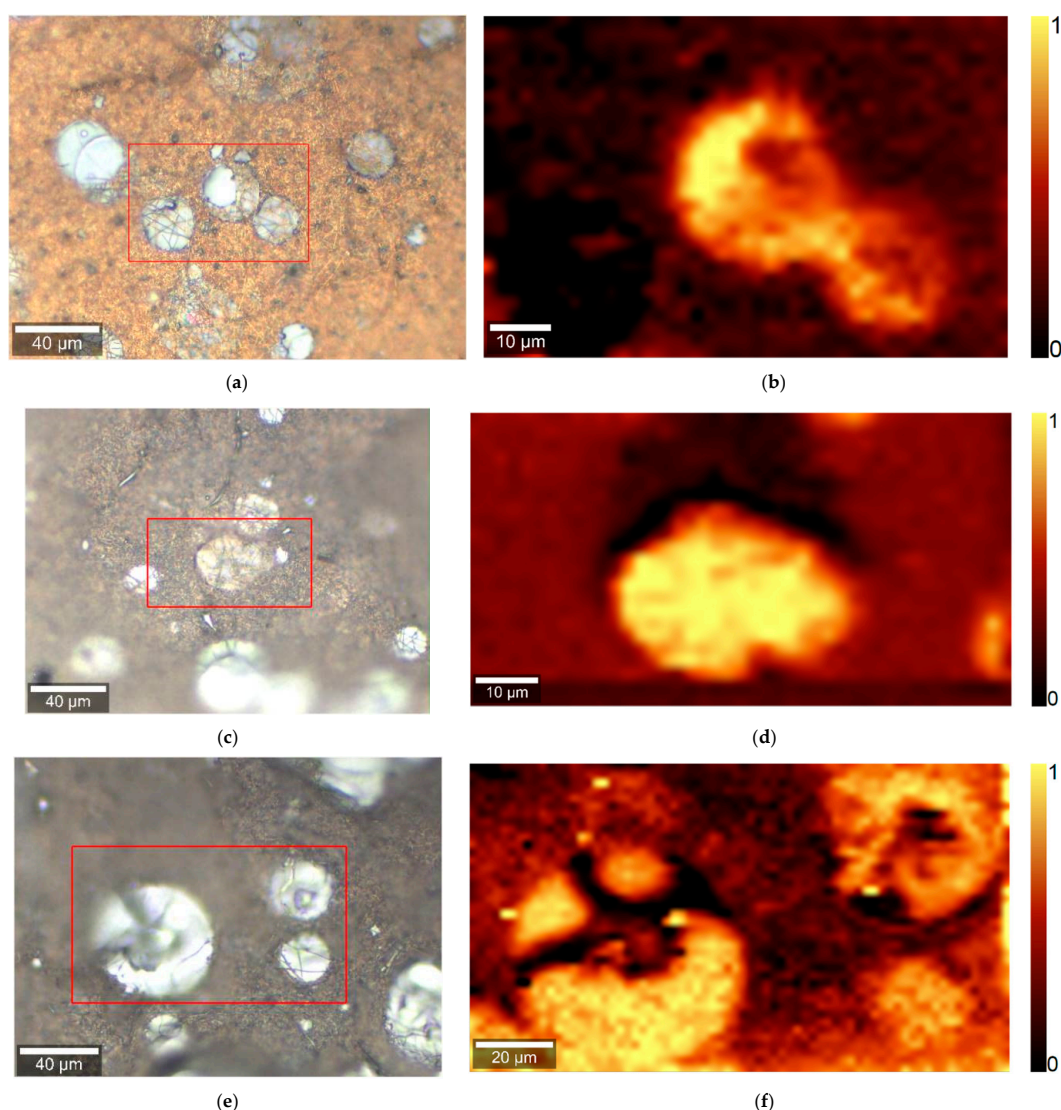

Figure 18. Microscopic images and Raman false-color images, taken in the marked areas, of PAN, taken on (**a**,**b**) PAN stabilized; (**c**,**d**) PAN carbonized; (**e**,**f**) PAN:PEO 9:1 carbonized. Regions with higher D/G ratios are shown in yellow.

In addition, the as-spun, stabilized, and carbonized samples (pure PAN and PAN:PEO 9:1, 300 kDa) were investigated by XRD (Figure 19). All XRD patterns show a broad

diffraction peak of molecular short-range order in the range between 15 and 35°, which is characteristic of amorphous polymers or amorphous regions in semi-crystalline polymers.
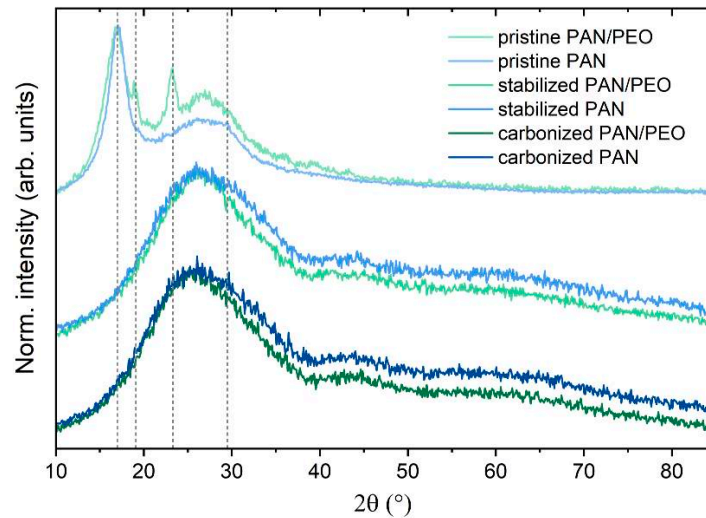

Figure 19. XRD patterns of pristine, stabilized, and carbonized nanofibers made of PAN and a PAN/PEO blend. The dashed lines show the main diffraction peaks.

The XRD patterns of the untreated PAN and PAN/PEO nanofibers show clearly identifiable diffraction peaks, which can be assigned to the respective polymers in good agreement with the published literature (17° for PAN and 19.1° and 23.3° PEO) [56,57]. Stabilization leads to amorphization, which is indicated by the disappearance of sharp diffraction peaks. Progressive carbonization and cyclization of the molecular structure lead to a gradual increase in long-range order, which gradually narrows the diffraction peaks towards a semi-crystalline hard carbon structure. The characteristic diffraction peaks, which only fully appear at higher temperatures, are [002] at about 22.2° (26.5° for graphite) and [100] at about 43.5° [58].

Finally, the carbon yield as well as the mass ratios gained after stabilization and carbonization only are depicted in Figure 20. Firstly, the mass ratio after stabilization depends strongly on the PEO content (Figure 20a), as expected, showing that PEO is largely degraded during the stabilization process, as expected. On the other hand, the pure carbonization process shows very similar values for all samples, with a slight tendency towards higher values for samples with more PEO. This may be attributed to a lower degree of carbonization in the non-fibrous areas with their lower surface-to-volume ratio.
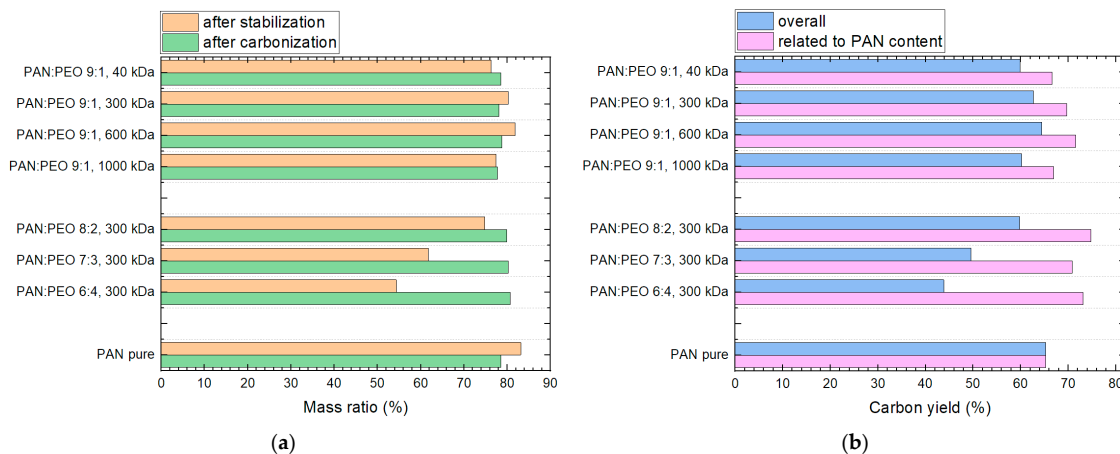

Figure 20. (**a**) Mass ratio of samples under investigation after stabilization and carbonization only; (**b**) carbon yield calculated for the overall sample mass and normalized to the PAN content.

The overall carbon yield (Figure 20b) is correspondingly larger for samples with a lower amount of PEO, i.e., highest for pure PAN and lowest for the 6:4 sample. On the other hand, if the mass after carbonization is related to the mass of PAN in the sample, all samples show higher normalized carbon yields than the pure PAN sample, indicating that the PEO is indeed partly carbonized.

This finding shows that more research is necessary on the stabilization and carbonization of PAN:PEO nanofiber mats, especially related to the stabilization process, to possibly find a more suitable process that enables stabilizing both polymers, e.g., by performing a first stabilization step at low temperatures under N_2 atmosphere, followed by typical temperatures for the stabilization of PAN in air. Alternatively, stabilization could be performed after fully washing the PEO out of the nanofiber mat blend; however, since no pores were visible in the nanofibers after washing, it can be assumed that further thermal treatment of the washed samples will not result in pore formation.

Finally, the unusual morphology of the 7:3 sample (first spinning process) indicates that either small temperature changes in the spinning chamber have a larger impact than expected, or even more spinning parameters have to be taken into account when results from needle-based electrospinning are planned to be upscaled by changing to wire-based or other needleless electrospinning techniques.

4. Conclusions

PAN:PEO nanofiber mats with different mass ratios and PEO molecular weights were electrospun by a wire-based device and partly watered, stabilized, and carbonized. While previous studies of needle-based electrospinning of similar solutions reported either smooth or porous nanofibers after carbonization, depending on the exact solution parameters, here we found smooth fibers combined with non-fibrous areas in the nanofiber mats as well as unexpectedly large fiber diameters for a PAN:PEO ratio of 7:3. These results show that transferring results from needle-based to needleless electrospinning is not always straightforward, and more research on this polymer blend system is necessary to identify all relevant solution and spinning parameters, which may influence the nanofiber and mat morphologies.

References

1. Oktay, B.; Kayaman-Apohan, N.; Erdem-Kurucu, S. Fabrication of nanofiber mats from electrospinning of functionalized polymers. *IOP Conf. Ser. Mater. Sci. Eng.* **2014**, *64*, 012011. [CrossRef]
2. Hanumantharao, S.N.; Rao, S. Multi-Functional Electrospun Nanofibers from Polymer Blends for Scaffold Tissue Engineering. *Fibers* **2019**, *7*, 66. [CrossRef]
3. Shetty, K.; Bhandari, A.; Yadav, K.S. Nanoparticles incorporated in nanofibers using electrospinning: A novel nano-in-nano delivery system. *J. Control. Release* **2022**, *350*, 421–434. [CrossRef] [PubMed]
4. Ahmadian, A.; Shafiee, A.; Aliahmad, N.; Agarwal, M. Overview of Nano-Fiber Mats Fabrication via Electrospinning and Morphology Analysis. *Textiles* **2021**, *1*, 206–226. [CrossRef]
5. Lee, J.Y.; Moon, S.J.; Lahann, J.; Lee, K.J. Recent Progress in Preparing Nonwoven Nanofibers via Needleless Electrospinning. *Macromol. Mater. Eng.* **2023**, *308*, 2300057. [CrossRef]
6. Mamun, A.; Klöcker, M.; Blachowicz, T.; Sabantina, L. Investigation of the Morphological Structure of Needle-Free Electrospun Magnetic Nanofiber Mats. *Magnetochemistry* **2022**, *8*, 25. [CrossRef]
7. Mamun, A.; Blachowicz, T.; Sabantina, L. Electrospun Nanofiber Mats for Filtering Applications—Technology, Structure and Materials. *Polymers* **2021**, *13*, 1368. [CrossRef]
8. Gul, A.; Gallus, I.; Sozcu, S.; Yalcinkaya, F. *Electrospun Nanofibrous Materials for Oil/Water Separation*; ACS Symposium Series; ACS Publications: Washington, DC, USA, 2022; Volume 1407, pp. 41–81.
9. Chen, S.X.; John, J.V.; McCarthy, A.; Xie, J.W. New forms of electrospun nanofiber materials for biomedical applications. *J. Mater. Chem. B* **2020**, *8*, 3733–3746. [CrossRef]
10. Gul, A.; Gallus, I.; Tegginamath, A.; Maryska, J.; Yalcinkaya, F. Electrospun Antibacterial Nanomaterials for Wound Dressings Applications. *Membranes* **2021**, *11*, 908. [CrossRef]
11. Langwald, S.V.; Ehrmann, A.; Sabantina, L. Measuring Physical Properties of Electrospun Nanofiber Mats for Different Biomedical Applications. *Membranes* **2023**, *13*, 488. [CrossRef]
12. Kailasa, S.; Bhargava Reddy, M.S.; Maurya, M.R.; Rani, B.G.; Rao, K.V.; Sadasivuni, K.K. Electrospun Nanofibers: Materials, Synthesis Parameters, and Their Role in Sensing Applications. *Macromol. Mater. Eng.* **2021**, *306*, 2100410. [CrossRef]
13. Song, J.L.; Lin, X.H.; Ee, L.Y.; Li, S.F.Y.; Huang, M.H. A Review on Electrospinning as Versatile Supports for Diverse Nanofibers and Their Applications in Environmental Sensing. *Adv. Fiber Mater.* **2023**, *5*, 429–460. [CrossRef] [PubMed]
14. Baghali, M.; Jayathilaka, W.A.D.M.; Ramakrishna, S. The Role of Electrospun Nanomaterials in the Future of Energy and Environment. *Materials* **2021**, *14*, 558. [CrossRef] [PubMed]
15. Dou, Y.B.; Zhang, W.J.; Kaiser, A. Electrospinning of Metal–Organic Frameworks for Energy and Environmental Applications. *Adv. Sci.* **2020**, *7*, 1902590. [CrossRef]
16. Azman, N.Z.N.; Mohamed, W.f.I.W.; Ramli, R.M. Synthesis and characterization of electrospun n-ZnO/n-Bi$_2$O$_3$/epoxy-PVA nanofiber mat for low X-ray energy shielding application. *Radiat. Phys. Chem.* **2022**, *195*, 110102. [CrossRef]
17. Chen, X.; Bi, Q.S.; Sajjad, M.; Wang, X.; Ren, Y.; Zhou, X.W.; Xu, W.; Liu, Z. One-dimensional porous silicon nanowires with large surface area for fast charge–discharge lithium-ion batteries. *Nanomaterials* **2018**, *8*, 12. [CrossRef]
18. Xiong, S.W.; Yu, Y.; Wang, P.; Liu, M.; Chen, S.H.; Yin, X.Z.; Wang, L.X.; Wang, H. Growth of AgBr/Ag$_3$PO$_4$ heterojunction on chitosan fibers for degrading organic pollutants. *Adv. Fiber Mater.* **2020**, *2*, 246–255. [CrossRef]
19. Liu, R.R.; Hou, L.L.; Yue, G.C.; Li, H.K.; Zhang, J.S.; Liu, J.; Miao, B.B.; Wang, N.; Bai, J.; Cui, Z.M.; et al. Progress of Fabrication and Applications of Electrospun Hierarchically Porous Nanofibers. *Adv. Fiber Mater.* **2022**, *4*, 604–630. [CrossRef]
20. Tian, L.D.; Ji, D.X.; Zhang, S.; He, X.W.; Ramakrishna, S.; Zhang, Q.Y. A Humidity-Induced Nontemplating Route toward Hierarchical Porous Carbon Fiber Hybrid for Efficient Bifunctional Oxygen Catalysis. *Small* **2020**, *16*, 2001743. [CrossRef]
21. Mailley, D.; Hébraud, A.; Schlatter, G. A Review on the Impact of Humidity during Electrospinning: From the Nanofiber Structure Engineering to the Applications. *Macromol. Mater. Eng.* **2021**, *306*, 2100115. [CrossRef]
22. Huang, L.W.; Bui, N.-N.; Manickam, S.S.; McCutcheon, J.R. Controlling electrospun nanofiber morphology and mechanical properties using humidity. *J. Polym. Sci. B Polym. Phys.* **2011**, *49*, 1734–1744. [CrossRef]
23. Gupta, D.; Jassal, M.; Agrawal, A.K. The electrospinning behavior of poly(vinyl alcohol) in DMSO–water binary solvent mixtures. *RSC Adv.* **2016**, *6*, 102947–102955. [CrossRef]
24. Russo, F.; Ursino, C.; Avruscio, E.; Desiderio, G.; Perrone, A.; Santoro, S.; Galiano, F.; Figoli, A. Innovative Poly (Vinylidene Fluoride) (PVDF) Electrospun Nanofiber Membrane Preparation Using DMSO as a Low Toxicity Solvent. *Membranes* **2020**, *10*, 36. [CrossRef] [PubMed]
25. Wortmann, M.; Frese, N.; Sabantina, L.; Petkau, R.; Kinzel, F.; Gölzhäuser, A.; Moritzer, E.; Hüsgen, B.; Ehrmann, A. New Polymers for Needleless Electrospinning from Low-Toxic Solvents. *Nanomaterials* **2019**, *9*, 52. [CrossRef]
26. Ma, G.P.; Liu, Y.; Peng, C.; Fang, D.W.; He, B.J.; Nie, J. Paclitaxel loaded electrospun porous nanofibers as mat potential application for chemotherapy against prostate cancer. *Carbohydr. Polym.* **2011**, *86*, 505–512. [CrossRef]
27. Ma, C.; Wu, L.Q.; Dirican, M.; Cheng, H.; Li, J.J.; Song, Y.; Shi, J.L.; Zhang, X.W. ZnO-assisted synthesis of lignin-based ultra-fine microporous carbon nanofibers for supercapacitors. *J. Colloid Interface Sci.* **2021**, *586*, 412–422. [CrossRef]
28. Zhang, L.F.; Aboagye, A.; Kelkar, A.; Lai, C.L.; Fong, H. A review: Carbon nanofibers from electrospun polyacrylonitrile and their applications. *J. Mater. Sci.* **2014**, *49*, 463–480. [CrossRef]

29. He, G.H.; Song, Y.H.; Chen, S.L.; Wang, L. Porous carbon nanofiber mats from electrospun polyacrylonitrile/polymethylmethacrylate composite nanofibers for supercapacitor electrode materials. *J. Mater. Sci.* **2018**, *53*, 9721–9730. [CrossRef]

30. Zhou, Z.P.; Wu, X.-F. Graphene-beaded carbon nanofibers for use in supercapacitor electrodes: Synthesis and electrochemical characterization. *J. Power Sources* **2013**, *222*, 410–416. [CrossRef]

31. Park, S.-H.; Jung, H.-R.; Kim, B.-K.; Lee, W.-J. MWCNT/mesoporous carbon nanofibers composites prepared by electrospinning and silica template as counter electrodes for dye-sensitized solar cells. *J. Photochem. Photobiol. A Chem.* **2012**, *246*, 45–49. [CrossRef]

32. Wang, M.-X.; Huang, Z.-H.; Shimohara, T.; Kang, F.Y.; Liang, K.M. NO removal by electrospun porous carbon nanofibers at room temperature. *Chem. Eng. J.* **2011**, *170*, 505–511. [CrossRef]

33. Yin, J.; Qiu, Y.J.; Yu, J. Onion-like graphitic nanoshell structured Fe–N/C nanofibers derived from electrospinning for oxygen reduction reaction in acid media. *Electrochem. Comm.* **2013**, *30*, 1–4. [CrossRef]

34. Zhang, L.F.; Hsieh, Y.-L. Carbon nanofibers with nanoporosity and hollow channels from binary polyacrylonitrile systems. *Eur. Polym. J.* **2009**, *45*, 47–56. [CrossRef]

35. Zhang, L.F.; Hsieh, Y.-L. Nanoporous ultrahigh specific surface polyacrylonitrile fibres. *Nanotechnology* **2006**, *17*, 4416. [CrossRef]

36. Yang, D.-S.; Chaudhari, S.; Rajesh, K.P.; Yu, J.-S. Preparation of Nitrogen-Doped Porous Carbon Nanofibers and the Effect of Porosity, Electrical Conductivity, and Nitrogen Content on Their Oxygen Reduction Performance. *ChemCatChem* **2014**, *6*, 1236–1244. [CrossRef]

37. Storck, J.L.; Hellert, C.; Brockhagen, B.; Wortmann, M.; Diestelhorst, E.; Frese, N.; Grothe, T.; Ehrmann, A. Metallic supports accelerate carbonization and improve morphological stability of polyacrylonitrile nanofibers during heat treatment. *Materials* **2021**, *14*, 4686. [CrossRef]

38. Storck, J.L.; Wortmann, M.; Brockhagen, B.; Frese, N.; Diestelhorst, E.; Grothe, T.; Hellert, C.; Ehrmann, A. Comparative Study of Metal Substrates for Improved Carbonization of Electrospun PAN Nanofibers. *Polymers* **2022**, *14*, 721. [CrossRef]

39. Theodosopoulos, G.V.; Zisis, C.; Charalambidis, G.; Nikolaou, V.; Coutsolelos, A.G.; Pitsikalis, M. Synthesis, Characterization and Thermal Properties of Poly(ethylene oxide), PEO, Polymacromonomers via Anionic and Ring Opening Metathesis Polymerization. *Polymers* **2017**, *9*, 145. [CrossRef]

40. Nirwan, V.P.; Al-Kattan, A.; Fahmi, A.; Kabashin, A.V. Fabrication of Stable Nanofiber Matrices for Tissue Engineering via Electrospinning of Bare Laser-Synthesized Au Nanoparticles in Solutions of High Molecular Weight Chitosan. *Nanomaterials* **2019**, *9*, 1058. [CrossRef]

41. Jiang, Y.L.; Wu, Q.Q.; Zheng, Y.R.; Fernández Blázquez, J.P.; Martinez-Hergueta, F.; Clark, J.H.; Guo, J.W.; Yue, H.B. Electro-spinning Fabrication, Structural Analysis, Thermomechanical, Lyophobic, and Biocompatible Properties of Cottonseed Protein Isolate/Poly(ethylene oxide) Composite Fiber Mats. *Macromolecules* **2024**, *57*, 2974–2987. [CrossRef]

42. Colín-Orozco, J.; Zapata-Torres, M.; Rodríguez-Gattorno, G.; Pedroza-Islas, R. Properties of Poly (ethylene oxide)/ whey Protein Isolate Nanofibers Prepared by Electrospinning. *Food Biophys.* **2015**, *10*, 134–144. [CrossRef]

43. Mahltig, B. High-Performance Fibres—A Review of Properties and IR-Spectra. *Tekstilec* **2021**, *64*, 96–118. [CrossRef]

44. Mólnar, K.; Szolnoki, B.; Toldy, A.; Vas, L.M. Thermochemical stabilization and analysis of continuously electrospun nanofibers. *J. Therm. Anal. Calorim.* **2014**, *117*, 1123–1135. [CrossRef]

45. Pucic, I.; Jurkin, T. FTIR assessment of poly(ethylene oxide) irradiated in solid state, melt and aqeuous solution. *Radiat. Phys. Chem.* **2012**, *81*, 1426–1429. [CrossRef]

46. Wen, S.J.; Richardson, T.J.; Ghantous, D.J.; Striebel, K.A.; Ross, P.N.; Cairns, E.J. FTIR characterization of PEO + LiN(CF$_3$SO$_2$)$_2$ electrolytes. *J. Electroanal. Chem.* **1996**, *408*, 113–118. [CrossRef]

47. Ramesh, S.; Yuen, T.F.; Shen, C.J. Conductivity and FTIR studies on PEO–LiX [X: CF$_3$SO$_3^-$, SO$_4^{2-}$] polymer electrolytes. *Spectrochim. Acta Part A Mol. Biomol. Spectrosc.* **2008**, *69*, 670–675. [CrossRef]

48. Kochuveedu, S.T.; Jang, Y.J.; Jang, Y.H.; Lee, W.J.; Cha, M.-A.; Shin, H.Y.; Yoon, S.H.; Lee, S.-S.; Kim, S.O.; Shin, K.; et al. Visible-light active nanohybrid TiO$_2$/carbon photocatalysts with programmed morphology by direct carbonization of block copolymer templates. *Green Chem.* **2011**, *13*, 3391–3405. [CrossRef]

49. Szabó, L.; Xu, X.T.; Ohsawa, T.; Uto, K.; Henzie, J.; Ichinose, I.; Ebara, M. Ultrafine self-N-doped porous carbon nanofibers with hierarchical pore structure utilizing a biobased chitosan precursor. *Int. J. Biol. Macromol.* **2021**, *182*, 445–454. [CrossRef]

50. Szabó, L.; Xu, X.T.; Uto, K.C.; Henzie, J.; Yamauchi, Y.; Ichinose, I.; Ebara, M. Tailoring the Structure of Chitosan-Based Porous Carbon Nanofiber Architectures toward Efficient Capacitive Charge Storage and Capacitive Deionization. *ACS Appl. Mater. Interfaces* **2022**, *14*, 4004–4021. [CrossRef]

51. Liu, J.; Tang, K.; Song, K.P.; van Aken, P.A.; Yu, Y.; Maier, J. Electrospun Na$_3$V$_2$(PO$_4$)$_3$/C nanofibers as stable cathode materials for sodium-ion batteries. *Nanoscale* **2014**, *6*, 5081–5086. [CrossRef]

52. Wortmann, M.; Layland, A.S.; Frese, N.; Kahmann, U.; Grothe, T.; Storck, J.L.; Blachowicz, T.; Grzybowski, J.; Hüsgen, B.; Ehrmann, A. On the reliability of highly magnified micrographs for structural analysis in materials science. *Sci. Rep.* **2020**, *10*, 14708. [CrossRef] [PubMed]

53. Sabantina, L.; Rodríguez-Cano, M.Á.; Klöcker, M.; García-Mateos, F.J.; Ternero-Hidalgo, J.J.; Mamun, A.; Beermann, F.; Schwak-enberg, M.; Voigt, A.-L.; Rodríguez-Mirasol, J.; et al. Fixing PAN Nanofiber Mats during Stabilization for Carbonization and Creating Novel Metal/Carbon Composites. *Polymers* **2018**, *10*, 735. [CrossRef] [PubMed]

54. Arshad, S.N.; Naraghi, M.; Chasiotis, I. Strong carbon nanofibers from electrospun polyacrylonitrile. *Carbon* **2011**, *49*, 1710–1719. [CrossRef]

55. Park, C.-W.; Youe, W.-J.; Han, S.-Y.; Kim, Y.S.; Lee, S.-H. Characteristics of carbon nanofibers produced from lignin/polyacrylonitrile (PAN)/kraft lignin-g-PAN copolymer blends electrospun nanofibers. *Holzforschung* **2017**, *71*, 743–750. [CrossRef]

56. Shen, T.; Li, C.; Haley, B.; Desai, S.; Strachan, A. Crystalline and pseudo-crystalline phases of polyacrylonitrile from molecular dynamics: Implications for carbon fiber precursors. *Polymer* **2018**, *155*, 13–26. [CrossRef]

57. Vasanthan, N.; Shin, I.D.; Tonelli, A.E. Structure, conformation, and motions of poly (ethylene oxide) and poly (ethylene glycol) in their urea inclusion compounds. *Macromolecules* **1996**, *29*, 263–267. [CrossRef]

58. Wortmann, M.; Keil, W.; Brockhagen, B.; Biedinger, J.; Westphal, M.; Weinberger, C.; Diestelhorst, E.; Hachmann, W.; Zhao, Y.; Tiemann, M.; et al. Pyrolysis of sucrose-derived hydrochar. *J. Anal. Appl. Pyrolysis* **2022**, *161*, 105404. [CrossRef]